AD-A082 378 GENERAL DYNAMICS SAN DIEGO CALIF ELECTRONICS DIV F/G 20/14
WAVE PROPAGATION THROUGH AXIALLY-SYMMETRIC DIELECTRIC SHELLS,(U)
FEB 80 G TRICOLES, E L ROPE, R A HAYWARD N00019-78-C-0594
UNCLASSIFIED R-80-008 NL

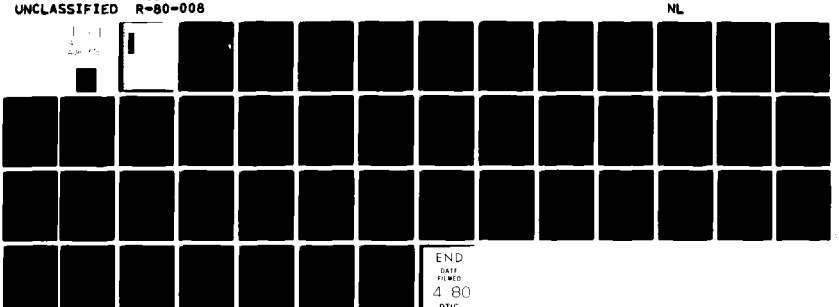

END
DATE FILMED
4 80
DTIC

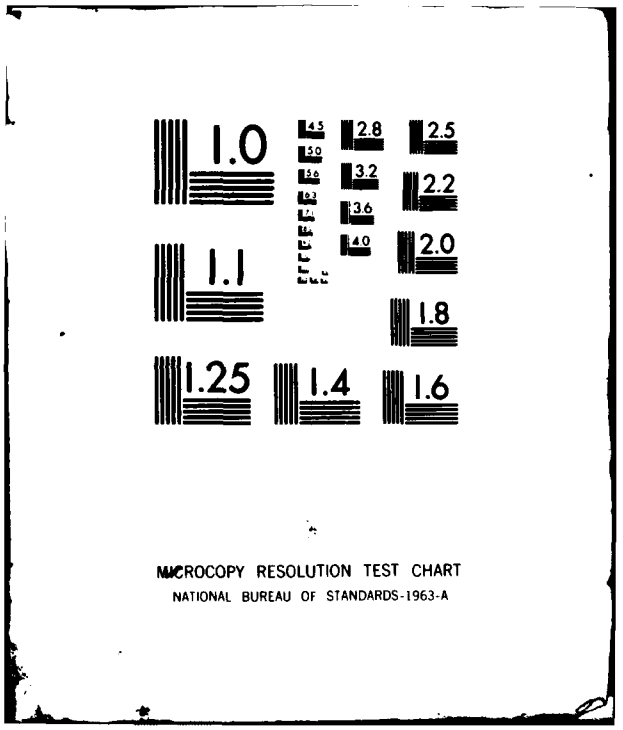
1.0
1.1
1.25
1.4
1.6
1.8
2.0
2.2
2.5
2.8
3.2
3.6
4.0
4.5
5.0
5.6
6.3
MICROCOPY RESOLUTION TEST CHART
NATIONAL BUREAU OF STANDARDS-1963-A

(12)

(14) Report No. R-80-956
February 1980

(6) WAVE PROPAGATION
THROUGH
AXIALLY-SYMMETRIC DIELECTRIC SHELLS

(9) Final Report

by

(10) G. Tricoles, E.L. Rope, R.A. Hayward

(11) Feb 80

(12) 47

Prepared for

U.S. Naval Air Systems Command
under
Contract No. (15) N00019-78-C-0594 new

APPROVED FOR PUBLIC RELEASE
DISTRIBUTION UNLIMITED

GENERAL DYNAMICS
Electronics Division
P.O. Box 81127, San Diego, California 92138 · 714-279-7301

CONTENTS

ILLUSTRATIONS

1. INTRODUCTION AND SUMMARY

1.1 INTRCDUCTION

Radomes can limit the performance of airborne radar and guidance systems by reducing guidance accuracy and radar range. This limitation persists despite continuing radome development because newer missiles fly faster and higher, and because newer threats require greater frequency bandwidths. In addition, the need for maximum radar range drives the antenna diameter to the maximum that fits within the radome; consequently, the antenna receives waves that are guided by the radome. These guided waves produce boresight errors. Our experiments have shown that the guided wave induced errors require radome correction techniques that differ from the usual method of small, local thickness variations.

The electromagnetic design of radomes and the correction of radome boresight error usually requires a long development period that includes much empirical work. Although analytical methods have been, and are being, developed, most methods are approximate. Unfortunately systematic error analyses are limited because radomes involve many factors and because the enclosed antenna influences performance.

Because of these limitations on radome design methods, interest exists in electronic compensation methods. Radome boresight error would be measured and stored in an on-board, digital memory, and these data would be applied as corrections during missile flight. This approach is attractive, but it has limitations. Obviously, adequate storage is required. The memory must be large since boresight error depends on gimbal angle, frequency, and wave polarization. Existing memories and processors seem capable of handling these variables within size limitations of missiles, but frequency and polarization sensors would be required. Cost impacts need study.

A potentially more serious problem is the temperature dependence of radome boresight error. This dependence involves many possible trajectories and the missile position within each trajectory. However, no accurate facility exists for measuring boresight error of heated radomes; this is an obstacle to electronic compensation. An alternative to electronic compensation is designing the radome for elevated temperatures. The radome would be somewhat thinner than for best room temperature performance. However, this alternative still requires high temperature measurements of boresight error for its evaluation, and it depends on accurate design methods.

Accurate radome design methods require accurate descriptions of wave propagation through the radome. This description must include the effects of frequency, polarization and the direction of the incident wave. The radii of curvature of the radome are

also a significant factor because they influence the wave types excited by an incident wave and the accuracy of approximate descriptions. Typical radii range from less than one to several wavelengths.

This report describes a continuing study of wave propagation through dielectric shells. Emphasis this year was on axially symmetric shells such as hollow cylinders. Last year we considered the hollow wedge, which is a two-dimensional radome, and the flat slab, which is a building block of a wedge and a local approximation to a shell.[1*] Quantitative data were given on phase shifts caused by refraction and plane wave propagation through the dielectrics; in addition some guided wave properties were determined. The analytical method used was the moment method[2, 3].

1.2 SUMMARY

Section 2 describes a technique estimating the amplitude and phase of guided waves excited on finite dielectric slabs by incident plane waves. The procedure is based on the moment method, but it extends that method by postulating an explicit form for the guided waves and solving for the guided wave amplitudes. The method solves for the two guided waves that travel in opposite directions parallel to the slab. Experiment verified the technique.

Section 3 describes nearfield scattering by a finite, solid, dielectric cylinder. Incidence was broadside. The procedure extends the theory originally developed by Richmond. It identifies the effects from the ends of the cylinder. Experiment verified the procedure for polarization parallel or perpendicular to the cylinder.

Section 4 describes a new technique for nearfield scattering by a hollow dielectric cylinder. The moment method was used but the cells were finite angular sectors. This is a new shape. Singularities of integrands were integrable. Experiment verified our approximate theory, especially when a correction for the pattern of the probe antenna was utilized.

*References are given in Section 5.

2. FINITE DIELECTRIC SLAB: GUIDED WAVE AMPLITUDE

2.1 INTRODUCTION

This section describes an application of the moment method to determining the guided wave magnitude on a finite dielectric slab. Reference 1 presented a moment method analysis of flat slabs, and it gave experimental checks. The method will be used in this report, but only a brief summary of the theory is included.

2.2 THEORY

Let us represent the field within the slab as a sum of four waves, which, in the co-ordinate system of Figure 2-1, are as follows:

1) A plane wave transmitted into the slab: $Te^{ik_x x}$,
2) A reflected plane wave: $Re^{ik_x x}$,
3) A slab-guided wave: $Ae^{ik_g x}$,
4) A reflected slab-guided wave: $Be^{-ik_g x}$,

At the slab midplane, Y equals zero; thus the field is

$$E(y = 0) = Se^{ik_x x} + Ae^{ik_g x} + Be^{-ik_g x}, \qquad (2\text{-}1)$$

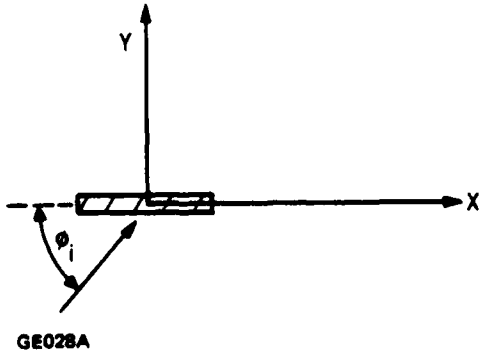

Figure 2-1. Co-ordinates for a Slab

where by assumption S is T +R, and T and R are respectively the complex-valued transmittance and reflectance of a flat dielectric sheet for plane waves. In addition, k_x is $(2\pi/\lambda) \sin \alpha$, with λ the wavelength and α the incidence angle, and k_g the propagation constant of a wave guided by an infinite slab.[2] We seek A and B.

The total field in a slab can be accurately determined with the moment method. Because that theory, extensive calculations, and measurements were given in Reference 1 through 3, we only summarize the method here. The moment method starts by dividing a slab into a set of N parallel cylinders and assuming the field constant within any cell. An integral equation for scattering relates the unknown total field E^T, the incident field E^I, and the scattered field E^S, so that

$$E^T - (ik^2/4)(\kappa - 1) \iint E^T (x', y') H_o^{(1)} (k\rho)\, dx'\, dy' = E^I, \qquad (2\text{-}2)$$

where $H_o^{(1)}$ is a Hankel function, κ is dielectric constant, and ρ is distance between observation and integration points. Equation 2-2 is evaluated at the center of each cell, with the integral extending over all cells, to produce N simultaneous, linear algebraic equations. The result is that

$$\sum_{n=1}^{N} C_{mn} E_n^T = E_m^I, \qquad (2\text{-}3)$$

for $1 \le m \le N$.

To determine A and B, combine Equations 2-1 and 2-3 and use Snell's law. Thus,

$$S\sum C_{mn} e^{ik_x x_n} + A\sum C_{mn} e^{ik_g x_n} + B\sum C_{mn} e^{-ik_g x_n} = e^{ik_x x_m}, \qquad (2\text{-}4)$$

for m equal 1 through N. Now N can be large. Its value depends on the size of the slab because cylinder radius is limited by the assumption that the field is constant. Although N is large, we have only two unknowns (A and B) because these guided wave amplitudes were assumed constant. Actually A and B could depend on x. In this case we would have N values of A and N values of B. However, if A and B vary slowly with x, it seems reasonable to consider successive pairs of equations in Equation 2-4 and to solve each pair for a value of A and a value of B. The solution is of course approximate because higher order modes can exist, and even the dominant slab mode may not be fully excited near an edge.

To evaluate A and B requires first evaluating the co-efficients C_{mn} and then solving successive pairs from Equation 2-4. For m and m+1 we obtain

$$A = [r_m - s'_m r_{m+1} (s'_{m+1})^{-1}] [s_m - s'_m s_{m+1} (s'_{m+1})^{-1}], \quad (2\text{-}5)$$

where

$$s_m = \sum C_{mn} e^{ik_g x_n}, \quad (2\text{-}6)$$

$$s_{m+1} = \sum C_{m+1,n} e^{ik_g x_n}, \quad (2\text{-}7)$$

$$s'_m = \sum C_{mn} e^{-ik_g x_n}, \quad (2\text{-}8)$$

$$s'_{m+1} = \sum C_{m+1,n} e^{-ik_g x_n}, \quad (2\text{-}9)$$

$$r_m = e^{ik_x x_m} - S \sum C_{mn} e^{ik_x x_n} \quad (2\text{-}10)$$

$$r_{m+1} = e^{ik_x x_{m+1}} - S \sum C_{m+1,n} e^{ik_x x_n}. \quad (2\text{-}11)$$

In addition,

$$B = (r_{m+1} - A s_{m+1}) (s'_{m+1})^{-1} \quad (2\text{-}12)$$

2.3 COMPUTATION

To test the approximate solution we analyzed a slab, with dielectric constant 2.6, thickness 0.25", and length 4". Experimental verification for the slab was given in Reference 3. Although the existence of guided waves was established and magnitudes were estimated, no explicit values of A and B were given. Frequency was 9.375 GHz and polarization was perpendicular. Figure 2-2 shows computed values of A and B. We see that computed values of A increase with x for grazing incidence $\phi_i = 0$ (or $\alpha = 90°$), but A decreases with x for $\phi_i = 22.5°$. For the other values of ϕ_i, the values oscillate.

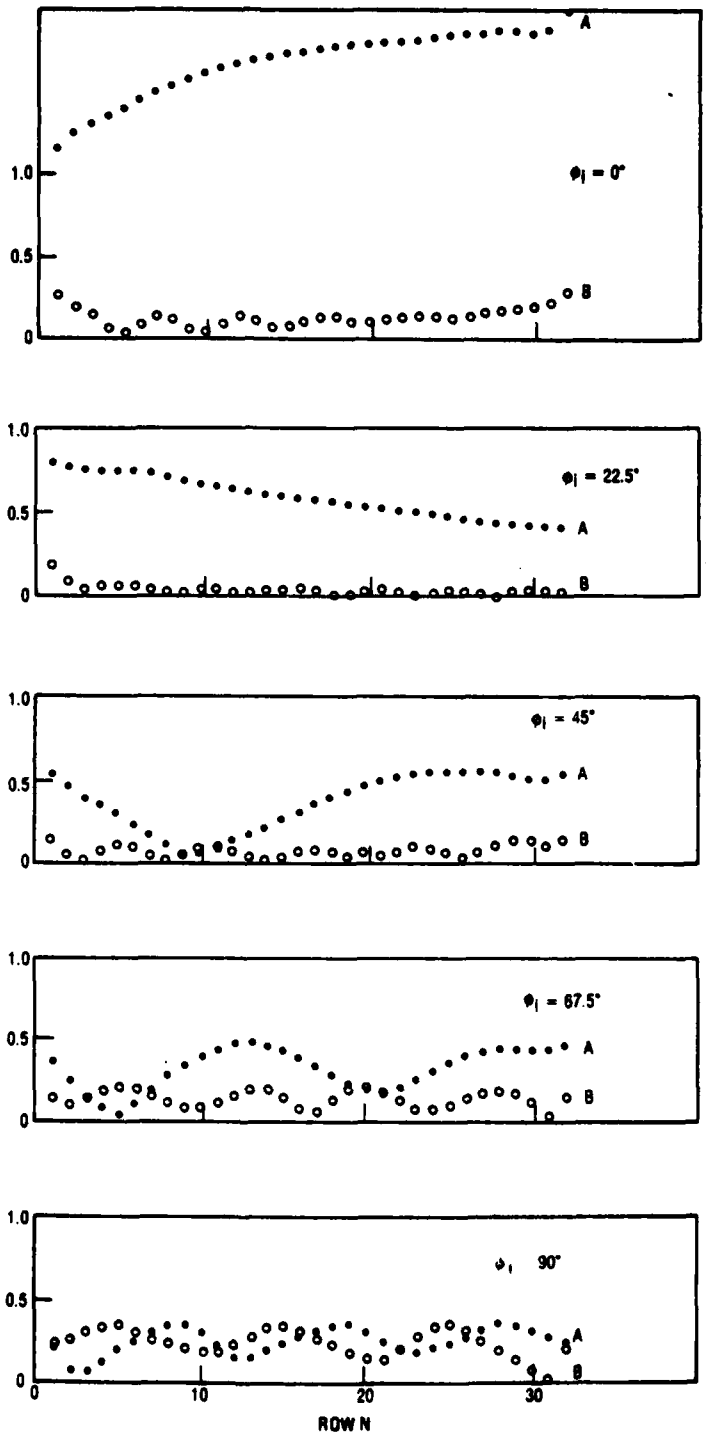

Figure 2-2. Guided Wave Amplitudes (Computed from Equations 2-5 and 2-12); $\phi_i = 0°$ is grazing incidence, and $\phi_i = 90°$ is normal. The x is N times the cell spacing.

2.4 MEASUREMENT

The field near the slab was measured with a microwave interferometer that utilized a dipole probe. Figure 2-3 shows an example of measured data for $\phi_i = 30°$; the probe was spaced 0.1" from the slab. We estimate guided wave amplitude A by first smoothing the curves to delete the reflected guided wave, amplitude B. We obtain two values of A, at minima and maxima on the condition that

$$E = T_p + Ae^{-vd} \tag{2-13}$$

where T_p is the plane wave power transmittance, v is the decay co-efficient for the field outside the slab and d is perpendicular distance. We utilize the extrema because at these features the two terms on the right hand side of Equation 2-13 are either in or out of phase. We then subtract T_p (which is easily calculated) from $|E|$, which is known from the measured graph of power $|E|^2$. After subtraction, the difference E - T_p is corrected by multiplying it by e^{vd}. We calculated v as 1.15π/inch from the theory of Reference 1. Figure 2-4 shows the values of A determined from the measured data for five incidence angles.

2.5 DISCUSSION

In Figure 2-4 the experimentally determined values of A fall within the envelope of the values of A computed by solving pairs of equations from Equations 2-4. This agreement verifies the approach to solving the guided wave excitation problem for a slab of finite length. The solution shows that A varies with position even for a single incidence angle. Our verification with experiment shows the model and technique are reasonable. We point out that we did not compare computed values of A at specific locations (values of x) with the experimental values at the same locations. However, the good agreement shown in Figure 2-4 substantiates the model in Equation 2-1* and the approximate pairwise solution of Equations 2-4.

In summary, we have utilized the accurate moment method as a step in a new procedure that estimates explicitly the magnitudes of guided waves on dielectric slabs. Although the moment method gave the total field, it did not identify constituent waves of distinct types. This identification may become useful in correcting radomes to reduce boresight error because the common radome practice of changing wall thickness to correct refractive errors seems ineffective for errors caused by guided waves. It seems possible that the method can be extended to replace A and B with functions of x while retaining the functional behavior given by Equation 2-1. Another possibility is to utilize N/2 values of A_n and N/2 values of B_n, on the assumption that A_n is identical for an adjacent pair of cells and similarly for B_n. We did not pursue a more

*This model was described in Reference 3.

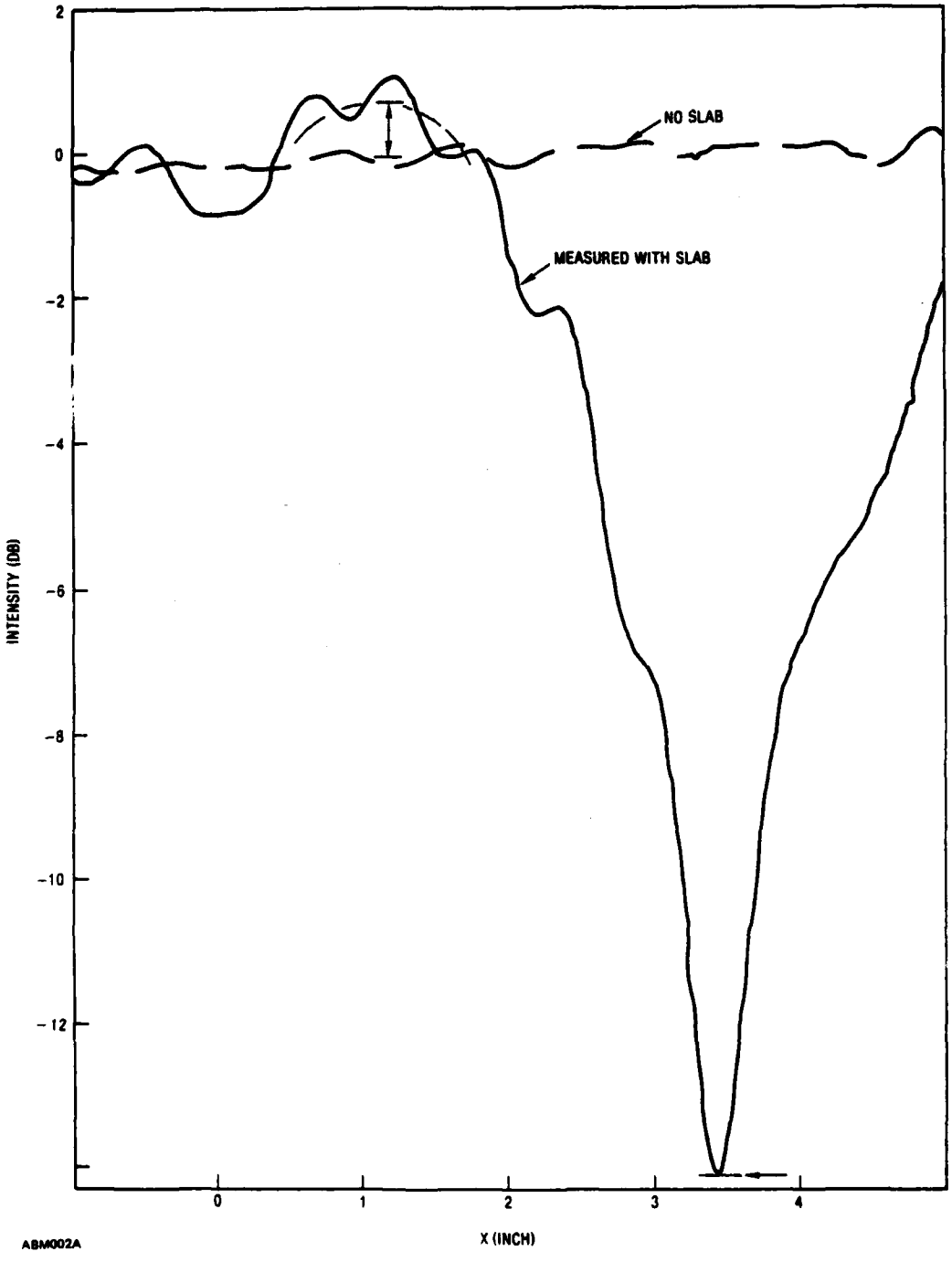

Figure 2-3. Measured Intensity Near Slab (Polarization Perpendicular, Dipole Probe 0.1" from Slab, Incidence Angle 60°; ϕ_i = 30°). The dashed extension of that measured with slab is a smoothed version. Arrows show the transmittance at peak intensity and the minimum value of intensity.

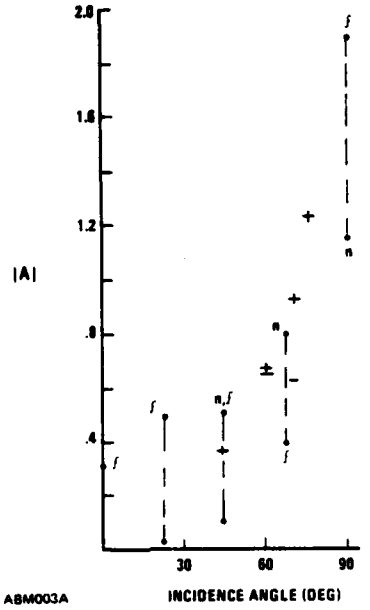

Figure 2-4. Guided Wave Amplitude (Computed from equation 2-5 (·); n denotes the edge nearest the source, f denotes edge further from source, measured at maxima (+), at minimum (-); data corrected by exp v d

detailed evaluation of the accuracy of this approach because the results in Figure 2-4 are reasonable and because the effects of curvature seemed more significant. The next sections introduce curvature; of course, they also consider finite objects.

3. NEARFIELD SCATTERING BY FINITE, SOLID CYLINDER

3.1 INTRODUCTION

This section describes nearfield scattering by a finite length, solid, dielectric cylinder. The solid cylinder was studied because it may be useful as an element for decomposing a hollow cylinder or an axially symmetric shell. The analysis extends that of Richmond for infinitely long cylinders.[3]

3.2 THEORY

The field scattered by a dielectric object can be expressed as a volume integral over polarization currents. The scattered field is

$$\underline{E}^s(\underline{r}') = (\underline{I}_1 + \nabla' \underline{I}_2)/4\pi \tag{3-1}$$

where

$$\underline{I}_1 = k^2 \int (\kappa - 1)\, g \underline{E}^T \, dv, \tag{3-2}$$

$$\underline{I}_2 = \int g \nabla \cdot [(\kappa - 1)\, \underline{E}^T] \, dv, \tag{3-3}$$

and $\underline{E}^T$ is the total field, g is r^{-1} expikr, and r is the distance between integration and observation points. The prime superscript (on the gradient operator and r') denotes the observation point.

The moment method determines $\underline{E}^T$, with the integral in Equation 3-1 and the relation that

$$\underline{E}^T - \underline{E}^s = \underline{E}^I \tag{3-4}$$

where $\underline{E}^I$ is the known, incident field. Equation 3-4 is an integral equation. It is reduced to a set of simultaneous algebraic equations by subdividing the scatterer into small cells for the purpose of evaluating Equations 3-3 and 3-4. The subdivision justifies assuming the field constant within each cell; this assumption simplifies the integration. This subdivision leads to a set of simultaneous equations from Equation 3-1.

The following sections describe the theory for calculating $\underline{E}^s$. To simplify notation let

$$\underline{E}^s(r') = \underline{E}^s_A + \underline{E}^s_s \tag{3-5}$$

where

$$\underline{E}^s_A = \underline{I}_1/4\pi\,, \tag{3-6}$$

and

$$E^s_s = \nabla' I_2/4\pi \tag{3-7}$$

3.2.1 EVALUATION OF $\underline{E}^S_A$

The integral $\underline{I}_1$ is expressed as a sum of integrals over discs like those in Figure 3-1. Assuming κ constant throughout the cylinder and that the field is constant within any one cell, we have from Equation 3-1 that

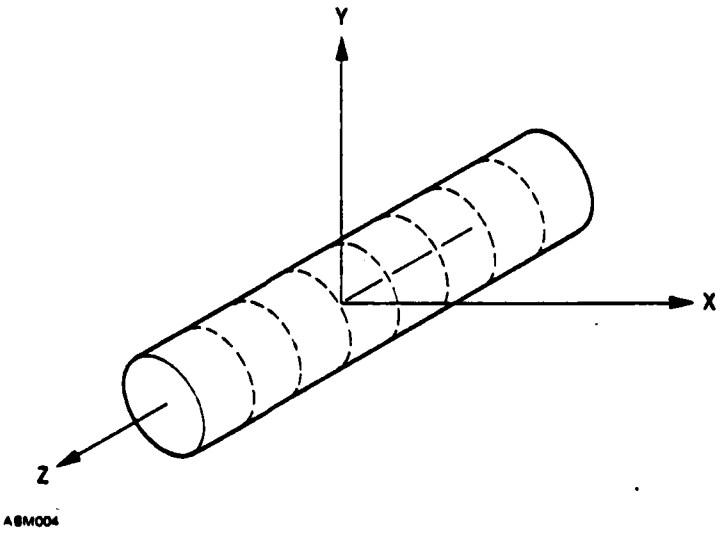

Figure 3-1. Subdivision of Cylinder Into Discs

$$\underline{I}_1 (\rho'_m, \phi'_m, z'_m) = k^2 (\kappa - 1) \sum_{n-1}^{N} \underline{E}_n^T \int g \, dv \,, \tag{3-8}$$

where $\underline{E}_n^T$ is the total electric field in the disc labelled n. Equation 3-1 leads to N simultaneous algebraic equations for m = 1, . . . N.

To evaluate the integrals in Equation 3-1 consider

$$r = \left[\rho^2 + \rho'^2 - 2\rho\rho' \cos(\phi - \phi') + (z - z')^2\right]^{1/2} . \tag{3-9}$$

Because the field is assumed constant within a disc, the field is evaluated at ρ'_m equal zero; the ϕ dependence is removed so the integral over ϕ given 2π. We have then that

$$\underline{I}_1 (z'_m) = 2\pi (\kappa - 1) \sum E_n^T \int_{z_n - \delta z}^{z_n + \delta z} \int_o^a \exp \left\{ ik \left[\rho^2 + (z_n - z'_m)^2\right]^{1/2} \right\} \tag{3-10}$$

$$\left[\rho^2 + (z_n - z'_m)^2\right]^{-1/2} dv$$

where a is the cylinder radius and each disc has thickness $2\delta z$. The integral over ρ can be done with the substitution that

$$u = \left[\rho^2 + (z'_m - z_n)^2\right]^{1/2}$$

to obtain

$$\underline{I}_1 = -i2\pi k (\kappa - 1) \sum \underline{E}_n \int_{z_n - \delta \grave{z}}^{z_n + \delta z} \left\{ \exp ik \left[a^2 + (z - z'_m)\right]^{1/2} - \exp ik (z - z'_m) \right\} dz \,. \tag{3-11}$$

There are two cases. First, $z_n \neq z'_m$; in this case expand the exponent

$$\left[a^2 + (z - z'_m)\right]^{1/2}$$

in a binomial series. The resulting functions have the form x^{-1} sinx where x is a linear in δz. For small δz x^{-1} sin x is approximately one so that

$$\underline{I}_1 = -i4\pi(\kappa-1)\,k\delta z \sum_{n=1}^{N} \left\{ \exp ik\left[a^2 + (z_n - z'_m)^2\right]^{1/2} - \exp ik\,|z_n - z'_m| \right\}. \tag{3-12}$$

In the second case $z_n = z'_m$; $z - z'_m$ is replaced by the variable ζ which ranges between δz and $-\delta z$. Again expanding the exponential in Equation 3-11, we obtain Fresnel integrals which we approximate by a small argument expansion, to obtain

$$\underline{I}_1 = 4\pi(\kappa-1)(ka)(k\delta z)\,\underline{E}^I_m. \tag{3-13}$$

Note that $\underline{I}_1$ has the same form for $\underline{E}$ polarized in the y direction and in the z direction.

The scattered field is found from Equations 3-12 and 3-13, and the definition in Equation 3-6.

3.2.2 $\underline{E}^S_S$ FOR THE FIELD PARALLEL TO THE CYLINDER AXIS

In this case, $\underline{E}$ has only a z component so Equation 3-3 gives

$$I_2 = \int g \frac{\partial}{\partial z}(\kappa-1)\,E_z\,dv. \tag{3-14}$$

Let the length of the cylinder be 2L. Then $(\kappa-1)$ is discontinuous with jumps at $z = \pm L$. We write it as $(\kappa-1)\,[H(z+L) - H(z-L)]$, where H is the Heaviside unit function. The partial differentiation leads to Dirac delta functions. We assume E_z varies slowly. Again decompose the integral into a sum of integrals over discs like in Figure 3-1, with the field constant in each disc, and integrate over z, to obtain

$$(\kappa-1)^{-1} I_2 = E_{z1} I_2(-L) - E_{zN} I_2(L) \tag{3-15}$$

where

$$I_2(L) = \int_0^{2\pi}\int_0^a r_-^{-1} (\exp ikr_-)\,\rho d\rho d\phi, \tag{3-16}$$

$$I_2(-L) = \int_0^{2\pi} \int_0^a r_+^{-1} (\exp ikr_+)\, \rho d\rho d\phi \ , \tag{3-17}$$

and

$$r_\pm = \left[\rho^2 + \rho'^2 - 2\rho\rho' \cos(\phi - \phi') + (L \pm z)^2\right]^{1/2} . \tag{3-18}$$

To evaluate the integrals in Equation 3-9, we expand the arguments of the exponentials to second order. Note that we cannot set ρ' to zero (as in the previous section) because of the gradient operator. After doing the integrals and the gradient operation we obtain

$$E^S_{zI2} = 1/2\,(\kappa - 1)\left\{\frac{a^2}{2} E_{z1}\left(ik - L_+^{-1}\right) L_+^{-1} e^{ikL+} - E_{zN}\left[1 - L_-\left(a^2 + L_-^2\right)^{-1/2}\right]\right\} \ , \tag{3-19}$$

and the scattered field from $I_2(-L)$ is

$$E^S_{zI2} = 1/2\,(\kappa - 1)\left\{E_{z1}\left[L_+\left(a^2 + L_+^2\right)^{-1/2} - 1\right] + \frac{a^2}{2} E_{zN}\left(ik - L_-^{-1}\right) e^{ikL_-}\right\} \tag{3-20}$$

where L_+ is $(L + z')$ and L_- is $(L - z')$.

The result of this subsection is that the integrations lead to two terms for the scattered field from Equation 3-13 and two terms from Equation 3-14. These terms arise from the δ functions associated with the ends of the cylinder. Recall $\partial E_z/\partial_z$ was omitted.

3.2.3 $\underline{E}^S_S$ FOR THE FIELD PERPENDICULAR TO THE CYLINDER AXIS

In this case the field has ρ and ϕ components so

$$I^S = \int g\left[\frac{\partial}{\partial\rho}(\kappa - 1) E_\rho + \frac{1}{\rho}\,\frac{\partial}{\partial\phi}(\kappa - 1) E_\phi\right] dv \tag{3-21}$$

As before, we assume that the field depends only on z; in addition $(\kappa - 1)$ is independent of ϕ. Therefore

$$I^S = \int g \frac{\partial}{\partial \rho} (\kappa - 1) E_\rho \, dv. \tag{3-22}$$

Let the function $(\kappa - 1)$ be $(\kappa - 1)$ [1 - H (a)] where now κ is the value in the dielectric and H (a) is the Heaviside function. Assume the field has only a y component so E_ρ is $E_y \sin\phi$. By decomposing the integration into the discs of Figure 3-1 we have

$$I_2 = -(\kappa - 1) E_{yn} \int g \sin\phi \; \delta(a) \, dv. \tag{3-23}$$

To do the integral first integrate on ρ and then introduce the variable $\phi - \phi' = \theta$. We obtain

$$I_2 = -(\kappa - 1) \, a \, \Sigma \, E_{yn} \int_{z_n - \delta z}^{z_n + \delta z} \int_{-\phi'}^{2\pi - \phi'} (\cos\phi' \sin\theta + \sin\phi' \cos\theta) \, g(a) \, d\theta \, dz \tag{3-24}$$

where g (a) is g in Equation 3-3 with

$$r = r(a) = [a^2 + \rho'^2 - 2a\rho' \cos\theta + (z - z')^2]^{1/2}. \tag{3-25}$$

The first term on the right side gives an integral equal zero because the integral is an odd function of θ. To evaluate the second term expand r (a) in a binomial series

$$r(a) \approx d - ad^{-1} \rho' \cos\underline{\theta} + \zeta d^{-1} \tag{3-26}$$

where d is $[(z_n - z'_m)^2 + a^2]^{1/2}$, and is $(z_n - z'_m)$. Recall z_n is at the center of the disc for which the integral is being done and z'_m is the observation point, at the center of one of the discs. The integration yields

$$I_2 = 2i \, \pi \, (\kappa - 1) \, \text{sinc} \, (k\delta z) \, \rho' \sin\phi' \, \Sigma \, E_{yn} \, d^{-1} \exp ikd \tag{3-27}$$

where sincx indicates $x^{-1} \sin x$. The scattered field follows from the gradient operation in Equation 3-1; the y component is

$$(\underline{E}^S)_y = \frac{i}{2} (\kappa - 1) \, ka^2 \, \delta z \, \text{sinc} \, (k\delta z) \, \Sigma \, E_{yn} \, d^{-1} \exp ikd \tag{3-28}$$

We see that the scattered field from the gradient of the scalar potential contains contributions from all discs. This result contrasts with the case for the field parallel to the cylinder. In that case there were only contributions from the ends for the gradient of the scalar potential.

3.2.4 ALGEBRAIC EQUATIONS FOR INTERNAL FIELDS

The algebraic equations result from the definition

$$\underline{E}^T - E^S = E^I \quad . \tag{3-29}$$

For the electric field parallel to the cylinder we have for m = 1, . . . N

$$\sum_{n=1}^{N} C_{mn} E_{zn} = E_m^I \, , \tag{3-30}$$

where

$$C_{11} = C_{NN} = 1 - p - B \, ,$$

$$C_{1N} = i\gamma\beta f_{IN} - A \, ,$$

$$C_{N1} = i\gamma\beta f_{NI} - A \, ;$$

for the other diagonal matrix elements,

$$C_{nn} = 1 - p \, ,$$

and for the remaining elements

$$C_{mn} = i\gamma\beta f_{mn}$$

where $\gamma = \kappa - 1$, $\beta = k\delta z$, $\alpha = ka$, $p = \alpha\beta\gamma$, and

$$f_{mn} = \exp ik\left[a^2 + (z_n - z_m)^2\right]^{1/2} - \exp ik\,|z_n - z_m| \, .$$

In addition

$$A = (\gamma a^2/4)\,[ik - (2L - \delta z)^{-1}]\,(2L - \delta z)^{-1} \exp ik\,(2L - \delta z)\,, \qquad (3\text{-}31)$$

and

$$B = (1/2)\,\gamma\left[\delta z\,(a^2 + \delta z^2)^{1/2} - 1\right]. \qquad (3\text{-}32)$$

For E^I perpendicular to the cylinder, the diagonal elements are

$$C_{nn} = 1 - p - h_{nn}$$

where

$$h_{nn} = i\,\gamma\alpha\,\delta z\, e^{ika}/2a$$

3.2.5 EXTERNAL FIELDS

The field outside a cylinder is found by evaluating Equation 3-1 with the values of E^T determined by solving Equation 3-30. The integrations are the volumes of the discs to preserve dimensional units of the field, not on set of points corresponding to disc centers. For the divergence we utilized finite differences.

First let us consider the contribution of the vector potential to the external, scattered field. From Equation 3-1,

$$\underline{E}^s_A\,(r') = \underline{I}_1/4\pi \qquad (3\text{-}33)$$

where

$$\underline{I}_1 = k^2 \int (\kappa - 1)\, g\, \underline{E}^T\, dv\,, \qquad (3\text{-}34)$$

and $\underline{E}^T$ is the total internal field, g is r^{-1} expikr with r the distance between integration and observation points, and κ is the dielectric constant. Equation 3-33 omits the term

$$\underline{E}^s_s = \nabla' \underline{I}_2/4\pi \qquad (3\text{-}35)$$

with the prime indicating differentiation on the observation coordinates where

$$\underline{I}_2 = \int g \nabla \cdot [(\kappa - 1) E] \, dv \tag{3-36}$$

The result from I_1 is for the q component (q = y or z)

$$E^s_{I_1}(x'_1 z') = \frac{1}{2}(ka)^2 \delta z (\kappa - 1) e^{ikx'} \sum E^T_q(z) e^{i\left[\pi (z_n - z')^2 / \lambda x'\right]} \left[x'^2 + (z_n - z')^2\right]^{-1/2} \tag{3-37}$$

For I_2 the integrations are different for E^I_y and E^I_z.

To evaluate $\underline{I}_2$ for E^I_y, in Equation 3-35 we utilize polar coordinates. So

$$\underline{I}_2 = \int g \left[\frac{\partial}{\partial \rho}(\kappa - 1) E_\rho \underline{1}_\rho + \frac{1}{\rho}\frac{\partial}{\partial \phi}(\kappa - 1) E_\phi \underline{1}_\phi\right] dv \, . \tag{3-38}$$

Because the dielectric cylinder has small diameter, we assume $\partial E\rho/\partial\rho$ is negligible. This assumption was also made in computing the internal field. Thus

$$\underline{I}_2 = -(\kappa - 1) \int g E_\rho \delta(a) \rho \, d\rho \, d\phi \, dz - (\kappa - 1) \int g (E_x \cos\phi + E_y \sin\phi) \, d\rho \, d\phi \, dz \tag{3-39}$$

The Dirac delta function comes from differentiating $(\kappa - 1)$. Now the incident field has only the E^I_y component, so we assume E_x is negligible. After some manipulation, we have

$$\underline{I}_2 = i\frac{3}{2} k (\kappa - 1) a^2 \int_{-L}^{L} \int_0^{2\pi} E_y e^{ik\sqrt{b}} b^{-1} \cos(\phi - \phi') \sin\phi \, d\phi \, dz \, , \tag{3-40}$$

where 2L is cylinder length and b is $\rho'^2 + (z - z')^2$. By stationary phase we integrate on z to obtain

$$E^s_s = i\frac{3}{8}(\kappa - 1)\sqrt{\pi}(ka)^2 \cos\phi' e^{ik\rho'} (k\rho')^{3/2} (F_+ + F_-) E_y \tag{3-41}$$

where $F_\pm$ is the Fresnel integral evaluated at $(2/\lambda\rho')^{1/2} (L \pm z')$.

For E_z^I, that is $\underline{E}^I$ parallel to the rod, the scattered field is associated with delta functions, at the ends of the cylinder, arising from the divergence operation. The result is assuming the field constant in the end cells

$$E_z^s(x', z') = \frac{1}{2} E_N (\kappa - 1) a^2 e^{ikD} D^{-1} \{LD^{-2} - ikLD^{-1}\}, \qquad (3\text{-}42)$$

where

$$D \text{ is } (\rho'^2 + L^2)^{1/2} .$$

for E_y^I,

$$E_y^s(x', z') = i(\kappa - 1) \frac{3}{8} \sqrt{\pi} (ka)^2 \cos\phi' e^{ik\rho} (k\rho)^{-3/2} (F_+ + F_-) E_y , \qquad (3\text{-}43)$$

if we assume the field is constant in the cylinder, where $F_\pm$ is the Fresnel integral evaluated at $\sqrt{2/\lambda\rho'}\,(L \pm z')$.

3.3 COMPUTATIONAL EXAMPLES

The formulas of Sections 3.2.4 and 3.2.5 were utilized to calculate the fields near a cylinder. The first step was to invert the matrix in Equation 3-30 to determine the total field within the cylinder. The second step was to compute the external field.

Figure 3-2 shows $|E^T|$ inside a dielectric cylinder for N = 26, with κ equal 2.6, diameter 0.139", length 1.9". The wavelength was 1.259", and the electric field was parallel to the cylinder axis. The figure gives $|E^T|$ computed according to the theory of Section 3.2.4 with A and B in Equations 3-31 and 3-32 set equal to zero and again for A and B evaluated according to these equations. We see that the effect of A and B is to change $|E^T|$ near the ends of the cylinder. Figure 3-2 also shows the exact value of $|E^T|$ for an infinitely long cylinder possessing diameter and dielectric constant equal to those of the finite cylinder.

The external field was computed first from the vector potential formula, Equation 3-37 with E^T the internal field computed from both the vector and scalar potentials. The total, external field was computed for E parallel to the cylinder axis for distance ρ' equal $\lambda/2$. See Figure 3-3. The total, external field for E perpendicular to the cylinder axis is shown in Figure 3-4 again for $\rho' = \lambda/2$. The effect of adding the contribution from the gradient of the scalar potential also is shown in Figures 3-3 and 3-4.

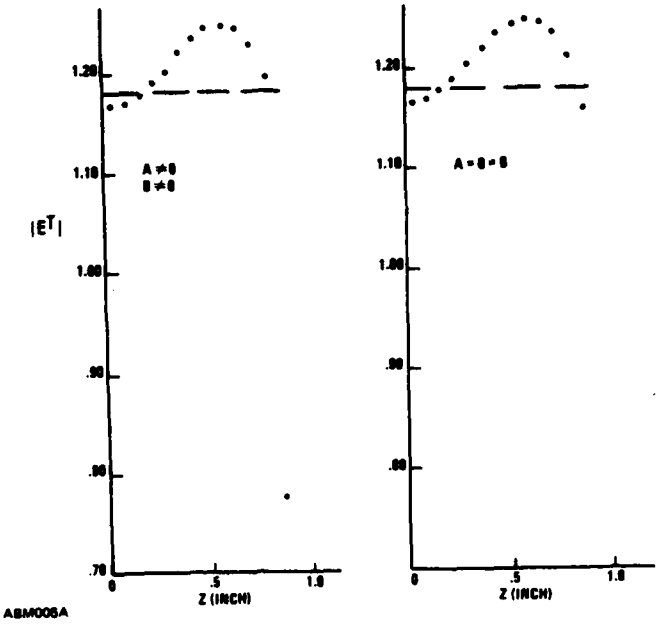

Figure 3-2. Total Internal Field $|E^T|$ inside cylinder, $\kappa = 2.6$, length 1.9", diameter 0.139" calculated by moment method. Exact solution for infinite cylinder (— —) $\lambda = 1.259$", N = 26.

3.4 MEASUREMENT

The field near the cylinder of Section 3-3 was measured with a dipole probe in a microwave interferometer. Reference 1 described apparatus and procedures. Figures 3-3 and 3-4 show measured data. The measurements were made with the cylinder suspended by Nylon threads. Additional data were given in Reference 1.

3.5 DISCUSSION

In general, the discrepancies between the measured and computed nearfield values of E^T are reasonably small and verify the theory, the mathematical approximations, and the numerical procedures. Figure 3-3 shows the scalar potential contribution negligibly changes the computed values for the field parallel to the rod. Discrepancies are small even without the scalar potential contribution. Figure 3-4 shows that the scalar potential contribution is significant for the electric field orthogonal to the rod.

The experimental data show $|E^T|^2$ is larger for the field parallel to the cylinder than for the field orthogonal. This result is intuitive. The phase values near the rod center are approximately equal for both cases. Near the ends of the cylinder phase decreases more rapidly for the parallel case.

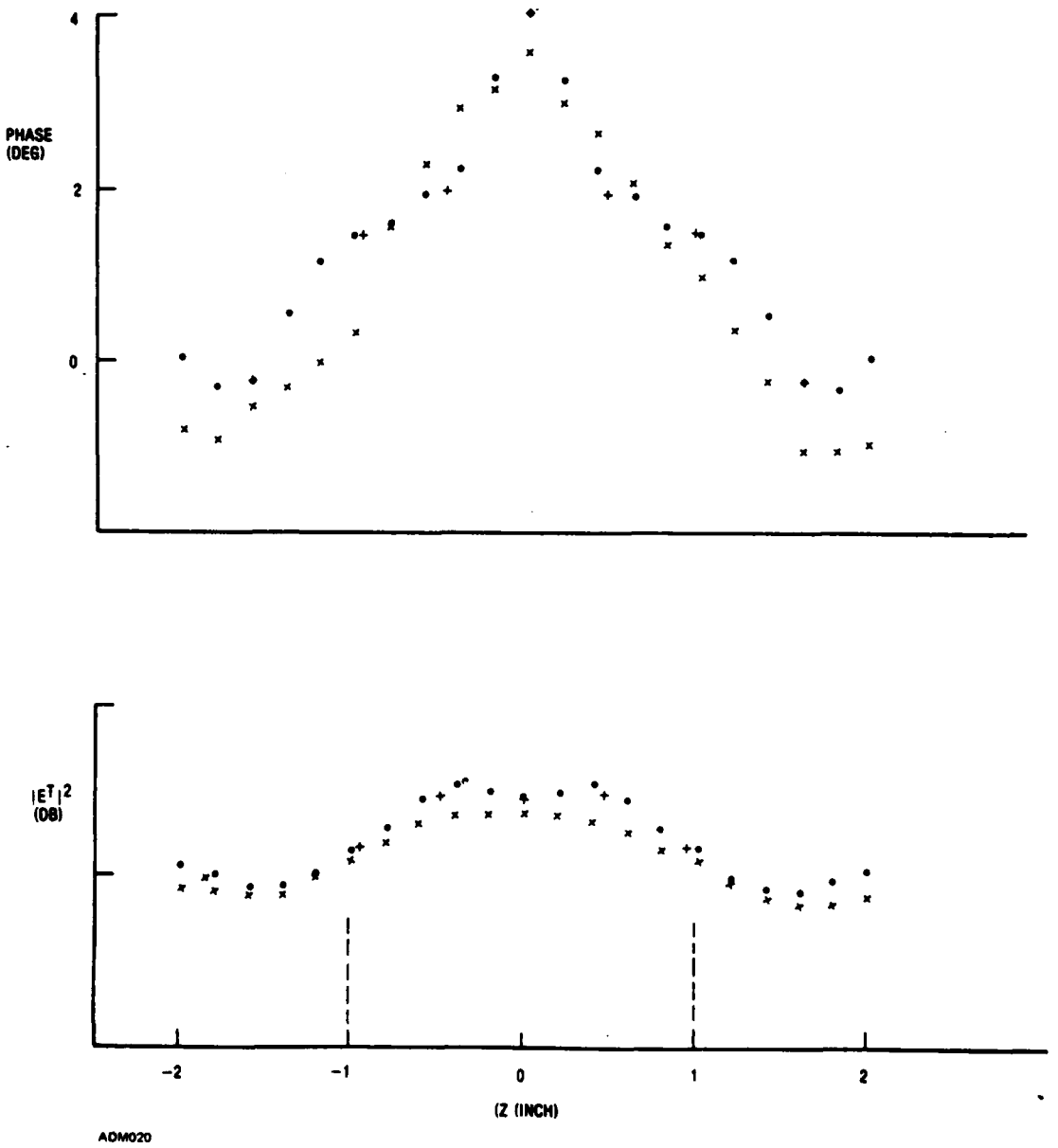

Figure 3-3. External Total field for 1.5 λ long rod; κ = 2.6; diameter = 0.139"; λ = 1.259 at x = 0.5 λ. Measured (x); computed from vector potential (·); from vector and scalar potentials (+). Electric field parallel to rod. The dashed lines show the ends of the cylinder.

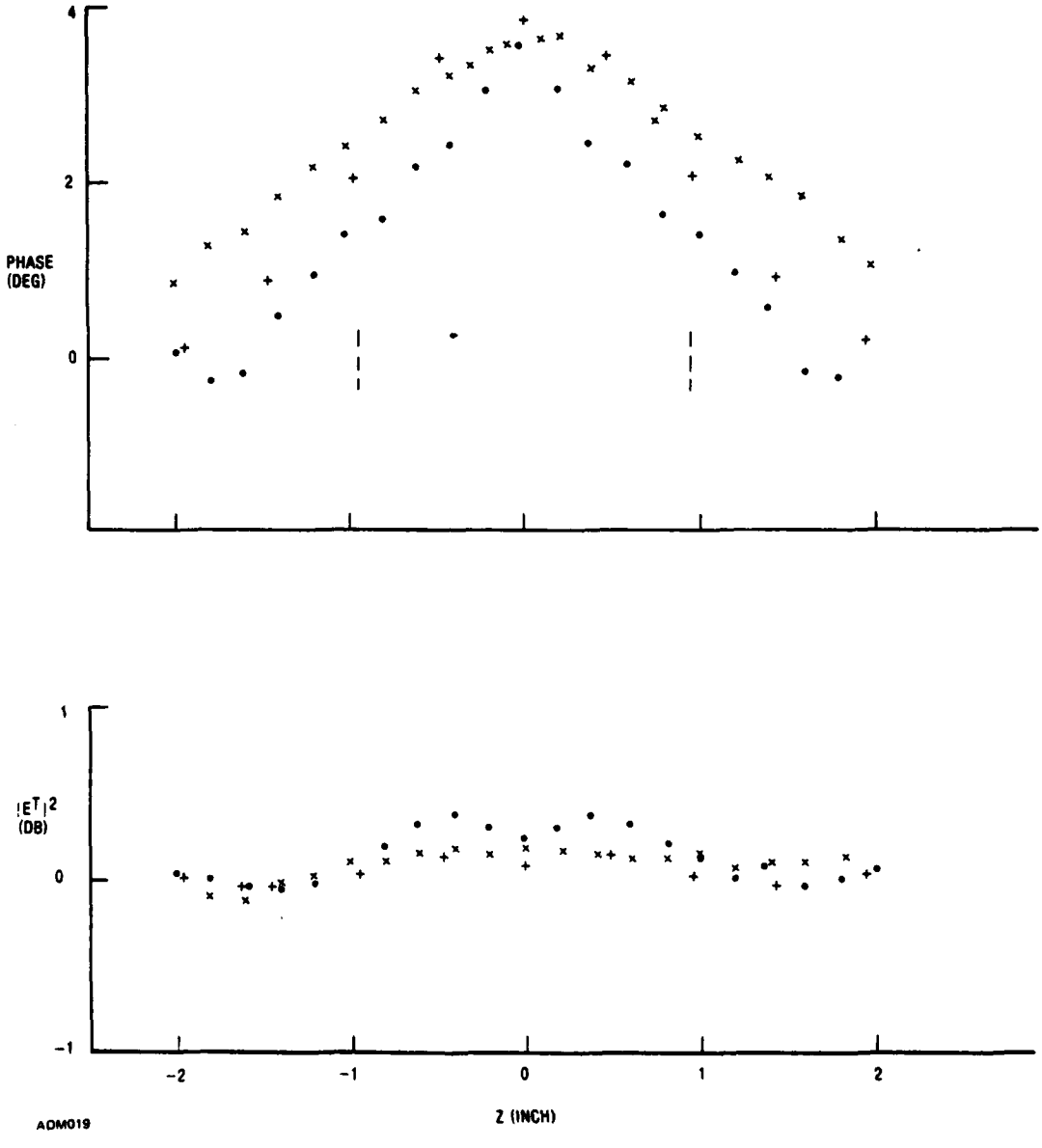

Figure 3-4. As in Figure 3-3, but for electric field perpendicular to rod.

4. NEARFIELD SCATTERING BY A HOLLOW DIELECTRIC CYLINDER

This section describes nearfield scattering by hollow dielectric cylinder.

4.1 THEORY

The integral equation for the electric field is obtained from the definition that the scattered field is

$$\underset{\sim}{E}^s = -\frac{\partial}{\partial t}\underset{\sim}{A} - \nabla' \Phi , \tag{4-1}$$

where the vector potential is a volume integral

$$\underset{\sim}{A} = -i\omega\rho_o \epsilon_o (4\pi)^{-1} \int (\kappa-1)\, g\, \underset{\sim}{E}\, dV , \tag{4-2}$$

the scalar potential is

$$\Phi = -(4\pi)^{-1} \int g\, \nabla \cdot (\kappa-1)\, \underset{\sim}{E}\, dV , \tag{4-3}$$

and g is r^{-1} expikr, with r the distance between observation and integration points κ is the dielectric constant, and the prime denotes differentiation on the observation point coordinates. In these formulas $\underset{\sim}{E}$ is the total field, which is unknown. The potentials arise from a polarization current

$$\underset{\sim}{j}_{pol} = -i\omega\epsilon_o (\kappa-1)\, \underset{\sim}{E} \tag{4-4}$$

and a polarization charge

$$\underset{\sim}{\rho}_{pol} = -\nabla \cdot (\kappa-1)\, \underset{\sim}{E} . \tag{4-5}$$

where the divergence is over the integration point coordinates.

The integral equation is

$$\underset{\sim}{E} - \underset{\sim}{E}^s = \underset{\sim}{E}^I \tag{4-6}$$

where $\underset{\sim}{E}^s$ is given by Equation (4-1) with A and Φ from Equations (4-2) and (4-3).

The integral equation is solved for the interior of the dielectric cylinder. The equation is changed to a set of simultaneous algebraic equations. The cylinder is divided into rings and subdivided into cells as in Figures 4-1, 4-2 and 4-3. The integral equation is evaluated at the center of each cell to generate as many equations as there are cells. At the center of a particular cell, labelled with index m, the integral equation for each rectangular component is

$$E_m - E_m^s = E_m^I$$

for $1 \leq m \leq N$, where N is the number of cells. E_m^s is a sum of contributions from all cells, so

$$E_m - \sum E_{mn}^s = E_m^I$$

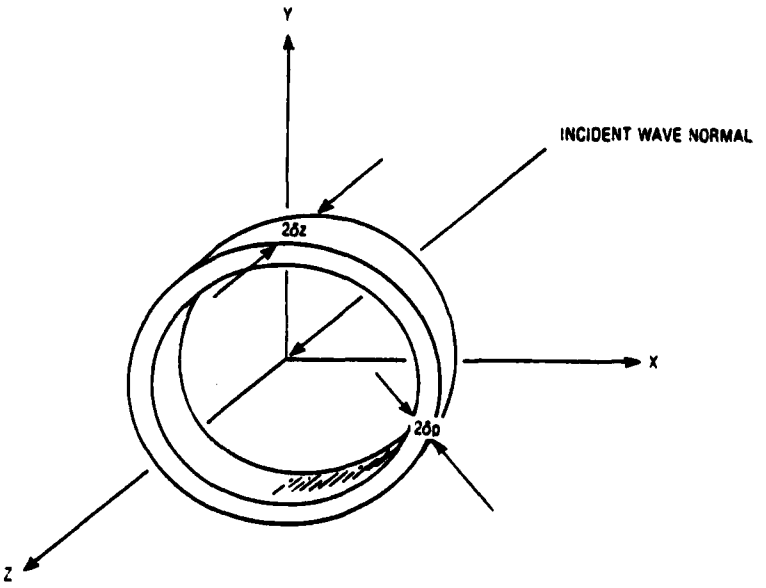

ADR002

Figure 4-1. Dielectric Ring and Coordinate System

This equation can be put into obvious matrix form by writing

$$E_m - \sum \left(E^s_{mn} / E_n \right) E_n = E^I_{m'}$$

or

$$\sum C_{mn} E_n = E^I_m$$

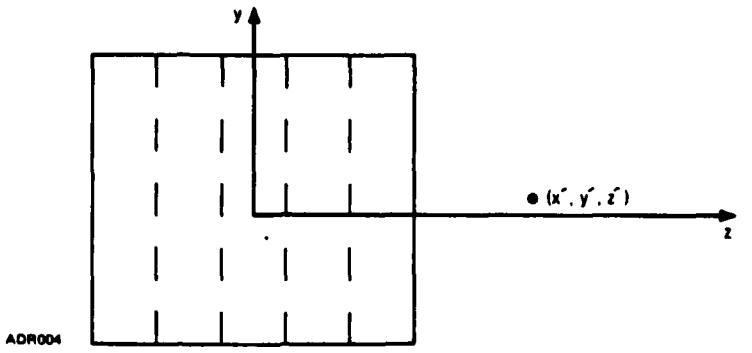

Figure 4-2. Subdivision of Hollow Cylinder Into Rings. An observation point has coordinates (x', y', z'); it may be inside or outside the cylinder.

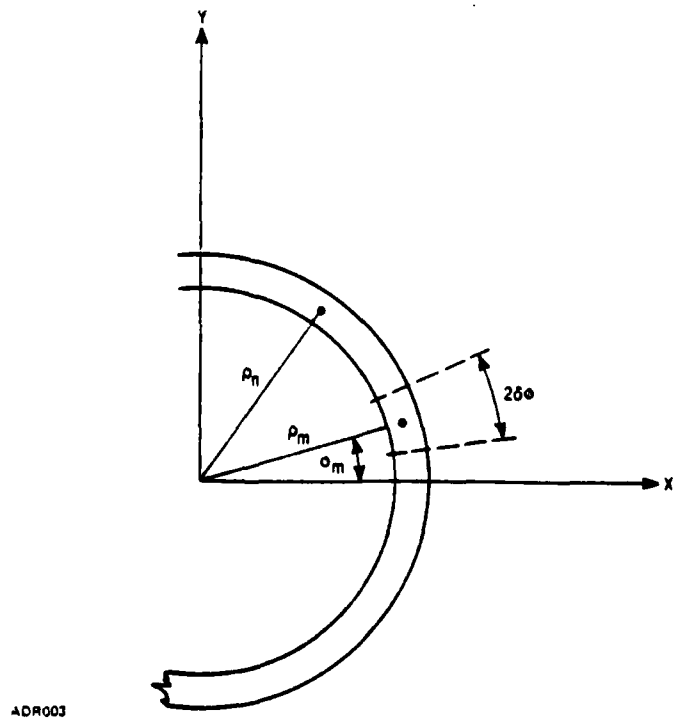

Figure 4-3. Coordinates for a Cell. A typical cell has dimensions as follows: radial $2\delta\rho$, circumferential $2\delta\phi$, and longitudinal $2\delta z$

where

$$C_{mm} = 1 - \left(E^s_{mm}/E_m\right),$$

and

$$C_{mn} = - E^s_{mn}/E_n$$

The next step is to evaluate the scattered fields E^s_{mn}. Formulas are derived in the following sections. Diagonal and off-diagonal matrix elements are separately given, and the vector and scalar potentials are separately evaluated.

4.2 SCATTERED FIELD FOR DIAGONAL ELEMENTS

4.2.1 VECTOR POTENTIAL

The scattered field from the vector potential is

$$\underline{E}^s = k^2 (\kappa-1) (4\pi)^{-1} \int g \underline{E} \, dV . \tag{4-7}$$

Let us assume horizontal polarization both incident and within the ring. This assumption may be valid if we consider thin rings and axial incidence. For the cell labelled m we have

$$E^s_{xm} = k^2 (\kappa-1) (4\pi)^{-1} \int g E_x \, dV_m \tag{4-8}$$

To simplify notation let

$$I_{Am} = \int g E_x \, dV_m \tag{4-9}$$

Since the integration extends only over the cell labelled m,

$$r = \left[\rho^2 + \rho_m^2 - 2\rho\rho_m \cos(\phi - \phi_m) + (z - z_m)^2\right]^{1/2} \tag{4-10}$$

with integration limits $\rho_m - \delta\rho \le \rho \le \rho_m + \delta\rho$, $z_m - \delta z \le z \le z_m + \delta z$, $\phi_m - \delta\phi \le \phi \le \phi_m + \delta\phi$. Introduce abbreviations $\theta = \phi - \phi_m$, $\zeta = z - z_m$, and $\sigma = \rho - \rho_m$. Then on assuming $\phi - \phi_m$ is small, we have

$$r \approx r_m = \left(\sigma^2 + \rho\rho_m\,\theta^2 + \zeta^2\right)^{1/2}, \tag{4-11}$$

so that

$$I_{Am} = \int_{-\delta z}^{\delta z}\int_{-\delta\phi}^{\delta\phi}\int_{-\delta\rho}^{\delta\rho} E_x\, r_m^{-1}\, e^{ikr_m}\,(\rho_m + \sigma)\cos\theta\, d\sigma\, d\theta\, d\zeta\,. \tag{4-12}$$

The factor cos θ in the integrand arises from first expressing the x-component of field in polar coordinates, expanding cos $(\theta + \phi_m)$ and sin $(\theta + \phi_m)$, and then using small angle approximations for sin θ and cos θ. Now assume r_m is small; that is, σ and ζ are small. Moreover, assume E_x is constant E_m in the cell. Thus we can expand the exponential, to obtain

$$I_{Am} = I_{Am}^{(1)} + I_{Am}^{(2)}\,; \tag{4-13}$$

where

$$I_{Am}^{(2)} = ik\,E_m \int_{-\delta z}^{\delta z}\int_{-\delta\phi}^{\delta\phi}\int_{-\delta\rho}^{\delta\rho} (\rho_m + \sigma)\cos\theta\, d\sigma\, d\theta\, d\zeta \tag{4-14}$$

This integral is, if we omit σ in $\rho_m + \sigma$,

$$I_{Am}^{(2)} = ik\,(8\,\delta z\,\delta\rho\,\rho_m\,\delta\phi)\,E_m \tag{4-15}$$

The factor in parentheses is the volume of the cell.

The term $I_{Am}^{(1)}$ is more complicated. We omit limits, which equal those in Equation (4-12)

$$I_{Am}^{(1)} = \iiint \left[(\rho_m + \sigma)\,\rho_m\,\theta^2 + \sigma^2 + \zeta^2\right]^{-1/2} (\rho_m + \sigma)\cos\theta\, d\sigma\, d\theta\, d\zeta\, E_m \tag{4-16}$$

The integral over ζ leads to a logarithmic function so

$$I_{Am}^{(1)} = \iint (\rho_m + \sigma)\cos\theta \log\left[(R+1)/(R-1)\right] d\sigma\, d\theta\, E_m \tag{4-17}$$

where R is $\left[1 + \left(s_+^2/\delta_z^2\right)\right]^{1/2}$, and

where s_+ is $\left[\sigma^2 + (\rho_m + \sigma)\,\rho_m\,\theta^2\right]^{1/2}$. Assuming $s_+^2 \ll \delta z^2$, to expand the square root, we obtain

$$I_{Am}^{(1)} = \iint (\rho_m + \sigma) \cos\theta \log\left\{4\delta z^2\, s_+^{-2}\left[1 + (s_+/2\delta z)^2\right]\right\} d\sigma\, d\theta\, E_m \qquad (4\text{-}18)$$

$$= \iint (\rho_m + \sigma) \cos\theta \log (2\delta/s_+)^2\, d\sigma\, d\theta\, E_m$$

$$+ \iint (s_+/2\delta z)^2\, (\rho_m + \sigma) \cos\theta\, d\sigma\, d\theta\, E_m$$

We assume that $\cos\theta \approx 1$ and $\sigma \ll \rho_m$ to carry out the integrals. We finally have that the x component of the scattered field is

$$I_{Am}^{(1)} = \pi s_2^2 \left[1 - \log (s/2\delta z)^2\right] + \rho_m \frac{\delta\rho\delta\phi}{3\delta z^2} s_2^2, \qquad (4\text{-}19)$$

where

$$s_2^2 = \delta\rho^2 + \rho_m^2\,\delta\phi^2$$

Equations (2-8), (2-13), (2-15), and (2-19) give the scattered field in the cell labelled m

$$E_{Am}^s = k^2 (\kappa - 1)\left\{i\frac{2}{\pi} k\,\delta z\,\delta\rho\,\rho_m\,\delta\phi + \frac{\rho m}{12\pi\delta z^2}\,\delta\rho\delta\phi\, s_2^2 + \frac{s^2}{4}\left[1 - \log (s_2/2\delta z)^2\right]\right\} E_m \qquad (4\text{-}20)$$

For brevity we omit the details of the integrations over σ and θ. The integral was done by integrating over local polar coordinates. In effect then our cells are small right circular cylinders not the truncated wedges defined by $\rho_m d\theta d\sigma$. This approximation procedure is described near the end of Paragraph 4.2.2.

4.2.2 SCALAR POTENTIAL

The scattered field from the scalar potential is

$$\underset{\sim}{E}_s^s = \frac{1}{4\pi} \nabla' I_2 \qquad (4\text{-}21)$$

where

$$I_2 = \int g \nabla \cdot (\kappa-1) \underset{\sim}{E} \, dV \ . \tag{4-22}$$

To represent the dielectric constant we use the unit step functions as functions of ρ only. That is, we shall understand,

$$(\kappa-1) = (\kappa-1) [H (\rho_m - \delta\rho) - H (\rho_m - \delta\rho)] \tag{4-23}$$

where on the right side $(\kappa-1)$ is a constant, but on the left κ is a function of ρ. Because we have assumed $E_z = 0$, it is unnecessary to specify the z dependence. Finally, κ is assumed independent of ϕ. Therefore

$$I_2 = \int \frac{e^{ikr}}{r} \nabla \cdot (\kappa-1) [H (\rho_m - \delta\rho) - H (\rho_m + \delta\rho)] \underset{\sim}{E} (\underline{1}_r \cos\phi - \underline{1}_\phi \sin\phi) \, dV \tag{4-24}$$

where $\underline{1}_r$ and $\underline{1}_\phi$ are unit vectors in the r and ϕ directions respectively.

We assume div E = 0, in the cell so

$$I_2 = (\kappa-1) E_m \left(I_2^{(1)} - I_2^{(2)} - I_2^{(3)}\right) , \tag{4-25}$$

where

$$I_2^{(1)} = \int g\delta (\rho_m - \delta\rho) \cos\phi \, dV_m , \tag{4-26}$$

$$I_2^{(2)} = \int g\delta (\rho_m + \delta\rho) \cos\phi \, dV_m , \tag{4-27}$$

$$I_2^{(3)} = \int g \cos\phi \, d\rho \, d\phi \, dz \ . \tag{4-28}$$

The first two integrals, $I_2^{(1)}$ and $I_2^{(2)}$, approximately cancel. To see this consider $I_2^{(1)}$. Assume kr is small and expand expikr. Thus

$$I_2^{(1)} = \int (r^{-1} + ik) \delta (\rho_m - \delta\rho) \cos\phi \, dV_m$$

The second term of the integrand, with factor ik, gives $-4ik\,(\rho_m - \delta\rho)\,\delta z\,\delta\phi\,\cos\phi_m$. This term is omitted because it approximately cancels the term $-4ik\,(\rho_m + \delta\rho)\,\delta z\,\delta\phi$ that arises from $I_2^{(2)}$. The first term, with factor r^{-1}, gives

$$I_2^{(1)} = \left(1 - \frac{\delta\rho}{\rho_m}\right)\cos\phi_m \int\left[(\zeta/\rho_m)^2 + (\delta\rho/\rho_m)^2 + \left(1 - \frac{\delta\rho}{\rho_m}\right)\theta^2\right]^{-1/2} \cos\theta\, d\theta\, d\zeta\,; \tag{4-29}$$

recall θ and ζ were defined earlier. Following integration on ζ we have

$$I_2^{(1)} = \left(1 - \frac{\delta\rho}{\rho_m}\right)\cos\phi_m \int(\ell n\, P_+ - \ell n\, P_-)\cos\theta\, d\theta\, d\zeta \tag{4-30}$$

where

$$P_\pm = \frac{q \pm \delta z}{\rho_m} + \frac{(\rho_m - \delta\rho)\,\theta^2}{2q} \tag{4-31}$$

and

$$q = \sqrt{\delta z^2 + \delta\rho^2} \tag{4-32}$$

The evaluation of $I_2^{(2)}$ proceeds in the same way. The result is that

$$I_2^{(2)} = \left(1 + \frac{\delta\rho}{\rho_m}\right)\cos\phi_m \int(\ell n\, Q_+ - \ell n\, Q_-)\cos\theta\, d\theta\, d\zeta \tag{4-33}$$

where

$$Q_\pm = \frac{(q \pm \delta z)}{\rho_m} + \frac{(\rho_m + \delta\rho)\,\theta^2}{2q} \tag{4-34}$$

Now consider

$$I_2^{(1)} - I_2^{(2)} = \left(1 - \frac{\delta\rho}{\rho_m}\right)\int \ell n\,(L_+/L_-)\, d\theta \tag{4-35}$$

where

$$L_{\pm} = \frac{s^2 - \delta z^2}{\rho_m^2} + \theta^2 + \frac{\rho_m^2 - \delta\rho^2}{4s^2}\,\theta^4 \pm \frac{\delta z}{s}\frac{\delta\rho}{\rho_m}\,\theta^2 . \tag{4-36}$$

Inspection of L_+/L_- shows that it tends to unit value for small θ. For example, at $\theta = 0$ the value is 1; for $\theta = 0.2$, the value is 1.046. Therefore the logarithm is small so the contributions of $I_2^{(1)}$ and $I_2^{(2)}$ from E^s_{Am} are omitted.

To evaluate $I_2^{(3)}$, expand the exponential, expikr, in the integrand as 1 + ikr. The first term is omitted because it is independent of the observation point coordinates so the ∇' operator yields zero. From the second term we obtain

$$I_2^{(3)} = \int r^{-1} \cos\phi \; d\rho \; d\phi \; dz \tag{4-37}$$

Again we use substitution $z - z_m = \zeta$, $\rho - \rho_m = \sigma$, $\phi - \phi_m = \theta$ to obtain

$$I_2^{(3)} = \cos\phi_m \iiint \left[\sigma^2 + (\rho_m + \sigma)\,\rho_m\,\theta^2 + \zeta^2\right]^{-1/2} \cos\theta \; d\rho \; d\theta \; d\zeta . \tag{4-38}$$

We assume θ is small so $\cos\theta \approx 1$. Integration on ζ gives

$$I_2^{(3)} = \cos\phi_m \iint \log\left\{\left[1 + \frac{(\rho_m + \theta)\,\rho_m\,\theta^2 + \sigma^2}{4\delta z^2}\right]\frac{4\delta_z^2}{\left[(\rho_m + \theta)\,\rho_m\,\theta^2 + \sigma^2\right]}\right\} d\sigma \; d\theta \tag{4-39}$$

Because wall thickness is much smaller than radius, we omit the term

$$\sigma\,\rho_m\,\theta^2/4\delta z$$

in the integrands. The integrations on σ and θ give

$$I_2^{(3)} = \pi\,\rho_m^{-1} \cos\phi_m \left[1 - \log\left(s_m/2\delta z\right)^2\right] s_m^2 + \frac{\delta\rho\;\delta\phi\;(\delta z)^{-2}}{3}\,s_m^2 \cos\phi_m \tag{4-40}$$

where

$$s_m^2 = \left(\delta\rho^2 + \rho_m^2\,\delta\phi^2\right).$$

To obtain the field apply the ∇' operator to $I_2^{(3)}$. The ρ and ϕ components are as follows:

$$\left(E^S_{\Phi m}\right)_\rho = -(\kappa-1)\left\{\frac{\delta\phi^2}{2}\left[1+\left(1-\log\left(\frac{s}{2}\right)^2\delta z^{-2}\right)\left(1-\frac{s^2}{2}\rho_m^{-2}\,\delta\phi^{-2}\right)\right.\right.$$

$$\left.\left.+\frac{\delta\rho\,\rho_m\,\delta\phi}{3\pi\,\delta z^2}\right]\cos\phi_m\right\}E_{xm} \qquad (4\text{-}41)$$

$$\left(E^S_{\Phi m}\right)_\phi = -(\kappa-1)\left(\frac{s}{2\rho_m}\right)^2\left\{\left[1-\log\frac{s^2}{2\delta z}\right]+\frac{\rho_m\,\delta\rho\,\delta\phi}{3\pi\delta z^2}\right\}\sin\phi_m\,E_{xm} \qquad (4\text{-}42)$$

From Equations (4-41) and (4-42), the contribution of the scalar potential to the x component of the scattered field is

$$E^S_{xm}(\Phi) = -(\kappa-1)\left\{\frac{\delta\phi^2}{2}\left[1+d\left(1-\frac{s^2}{2\rho_m^2\,\delta\phi^2}\right)+f\right]\cos^2\phi_m\right.$$

$$\left.+\left(\frac{s}{2\rho_m}\right)^2(d+f)\sin^2\phi_m\right\}E_{xm} \qquad (4\text{-}43)$$

where

$$d = 1-\log\left(\frac{s}{2}\right)^2 \qquad (4\text{-}44)$$

and

$$f = \rho_m\,\delta\rho\,\delta\phi/(3\pi\,\delta z)^2 \qquad (4\text{-}45)$$

4.3 SCATTERED FIELD FOR OFF-DIAGONAL ELEMENTS

4.3.1 VECTOR POTENTIAL

The scattered field at the cell centers results from a finite sum of integrals over cells like those in Figure 2-3. The vector potential gives for the x component

$$E^{s}_{Am} = k^{2} (4\pi)^{-1} (\kappa-1) \Sigma' E_{n} I , \tag{4-46}$$

where

$$I = \int g (\underline{1}_{\rho} \cos \phi - \underline{1}_{\phi} \sin \phi) \, d\phi , \tag{4-47}$$

and the prime suggests the sum excludes the term for n = m.

In g, set $\rho_n = \rho_m$; for small θ,

$$r = \left[2b\rho_m^2 + (z_n - z_m)^2 + 2\rho_m \, b\sigma + 2 (z_n - z_m) \zeta\right]^{1/2} \tag{4-48}$$

where b is $1 - \cos (\phi_n - \phi_m)$. The binomial expansion gives approximately that

$$r = \beta + \rho^{-1} [\rho_m \, b\sigma + (z_n - z_m) \zeta] , \tag{4-49}$$

where

$$\beta = \left[2b \, \rho_m^{\,2} + (z_n - z_m)^2\right]^{1/2} \tag{4-50}$$

With Equation (2-49),

$$I = \beta^{-1} e^{ik\beta} \int e^{ik \rho_m \, b\sigma/\beta} \, e^{ik (z_n - z_m) \zeta / \rho} (\rho_n + \sigma) \, d\sigma \, d\phi \, d\zeta . \tag{4-51}$$

$$= 8 \, \rho_m \, \delta\rho \, \delta z \, \delta\phi \, \beta^{-1} e^{ik\rho} \left\{1 - (1/6)\left(k \, \rho_m \, b\delta \, \rho\beta^{-1}\right)^2 - \frac{1}{6}\left[k (z_n - z_m) \, \delta z \, \beta^{-1}\right]^2\right\}$$

The higher terms have magnitudes much less than 1, so

$$I = 8\,\rho_m\,\delta\rho\,\delta z\,\delta\phi\,\beta^{-1}\,e^{ik\beta} \tag{4-52}$$

The scattered field is

$$E^s_{Am} = \frac{2}{\pi}(\kappa-1)\,k^2\,\rho_m\,\delta\rho\,\delta z\,\delta\phi\,\Sigma'\,E_{xn}\,\beta^{-1}\,e^{ik\beta} \tag{4-53}$$

4.3.2 SCALAR POTENTIAL

The derivation of matrix elements is slightly more general for this case because of the gradient on observation point coordinates. That is, the gradient operation ∇' is performed, after that set $\rho_m = \rho_n$. The distance in the expression for g is

$$r = \left[\rho + \rho_m^{\,2} - 2\rho\,\rho_m\cos(\phi - \phi_m) + (z - z_m)^2\right]^{1/2}, \tag{4-54}$$

Now let $z = z_n + \zeta$, $\rho = \rho_n + \sigma$ so that

$$r = \left[s^2 + 2\rho_n\,\sigma - 2\rho_m\,\sigma\cos(\phi_n - \phi_m) + 2\,(z_n - z_m)\right]^{1/2}, \tag{4-55}$$

where

$$s = \left(\rho_n^{\,2} + \rho_m^{\,2} + z_{nm}^{\,2} - 2\,\rho_n\,\rho_m\,\sigma\right)^{1/2} \tag{4-56}$$

The binomial expansion gives approximately that

$$r = s + \rho_n - \rho_m\cos(\phi_n - \phi_m) + z_{nm}\,s^{-1}\,\zeta\ . \tag{4-57}$$

Now consider $I_2^{(3)}$ of Equation (4-28). With r from Equation (4-57),

$$I_2^{(3)} = 8\,\delta\rho\,\delta\phi\,\delta z\,e^{iks}\,s^{-1}\cos\phi_n \tag{4-58}$$

if we approximate the sinc functions that result from integration by unit value.

From Equations (4-26) and (4-27),

$$I_2^{(1)} - I_2^{(2)} = -8\,\delta z\,\delta\phi\,\delta\rho\,e^{iks}\,s^{-1}\left\{1 + ik\rho_n\,[\rho_n - \rho_m \cos(\phi_n - \phi_m)]\,s^{-1}\right\}. \quad (4\text{-}59)$$

The scattered field from $I_2^{(3)}$ for the nth cell is

$$E_n^s\,I_2^{(3)} = -\frac{(\kappa-1)}{4\pi}\,E_{xn}\,\nabla' I_2^{(3)}$$

$$= -\frac{2}{\pi}(\kappa-1)\,\delta\rho\,\delta\phi\,\delta z\cos\phi_n\,E_n\,\nabla' e^{iks}\,s^{-1}\,E_{xn} \quad (4\text{-}60)$$

The differentiations are on ρ_m and ϕ_m. The x component is

$$E_x^s\,I_2^{(3)} = -\frac{2}{\pi}(\kappa-1)\,\delta\rho\,\delta z\,\delta\phi\cos\phi_n\,(ik - s^{-1})\,e^{iks}\,\rho_m\,s^{-2}\sin(\phi_n - \phi_m)\sin\phi_m\,E_{xn} \quad (4\text{-}61)$$

The gradient operation on $I_2^{(1)} - I_2^{(2)}$, gives two terms; in fact,

$$E_n^s\left(I_2^{(1)} - I_2^{(2)}\right) = E_n^s\,I_2^{(3)} + \Delta E_n^s \quad (4\text{-}62)$$

where

$$\Delta E_n^s = G_n\frac{e^{iks}}{s^2}\left\{s_{nm}\,s_m\left[2\rho_m^2\,s^{-2}\,b - 1 - i\,\rho_m^2\,bks^{-1}\right] + \frac{\rho_m}{s}\cos\phi_m\,b\left[2\,\rho_m\,bs^{-1} + (1-b) - ik\,\rho_m\,b\right]\right\} \quad (4\text{-}63)$$

with

$$s_{nm} = \sin(\phi_n - \phi_m) \quad \text{and} \quad s_m = \sin\phi_m\,.$$

4.4 EXTERNAL FIELDS

The field outside the dielectric region is found by evaluating Equations (4-7) and (4-21). The integration extends over the dielectric region. It can be done after the total field inside the dielectric is determined by solving the integral equation.

The field near a cylinder is evaluated to test the approximations in the derivations. The near field also is useful in understanding the effects of a dielectric cylinder or a radome on an antenna.

The field from the vector potential is

$$E^s(A) = i\omega A .$$

A measurement requires a probe. We consider a half-wave dipole and weight the contribution of each cell by the far-field pattern. To simplify the expressions, consider the field on the z-axis. The sector potential gives for the x component (from one ring)

$$\bar{E}^s(A_1) = (\kappa-1)\, k^2 (4\pi)^{-1} \int g\, E_x \cos\left(\frac{\pi}{2}\cos\theta\right) (\sin\theta)^{-1} \rho d\rho d\phi dz \qquad (4\text{-}64)$$

where the factor $\cos(\pi/2 \cos\theta)/\sin\theta$ is the far-field pattern of the probe. Consider the distance large enough so that

$$r = R + (a\sigma - a\rho\cos\phi - zz')\, R^{-1} \qquad (4\text{-}65)$$

where a is the mean radius of the cylinder and R is $(a^2 + z'^2)^{1/2}$. Furthermore approximate $\sin\theta$;

$$\sin\theta = 1 - (a/R)^2 \cos^2\phi \qquad (4\text{-}66)$$

To develop a simple formula we omit the dependence of E on ϕ and use an average value E_o. The integrations are elementary, so that

$$E^s(A_1) = 2(\kappa-1)\, k^2\, a\, \delta\rho\, \delta z\, E_o\, e^{ikR} R^{-1} \operatorname{sinc}(ka\,\delta\rho/R) \operatorname{sinc}(kz'\,\delta z/R)\, P$$

$$\left[1 - (a/2R)^2 \left(\frac{\pi^2}{4} - 1\right)\right] . \qquad (4\text{-}67)$$

P is $[1 - (a/2R)^2 (\pi^2/4 - 1)]$, the probe correction.

The field from the scalar potential is

$$E_x^s(\Phi) = (4\pi)^{-1} \nabla' \int g\, \nabla \cdot (\kappa-1)\, E_x\, dV . \qquad (4\text{-}68)$$

The procedures are like those in Section 4.2.2 and 4.3.2. So

$$E_x^s(\Phi) = -i(\kappa-1)\frac{a^2}{2\lambda}\frac{e^{ikR}}{R^2}E_o\int e^{ik(\ldots)}[\ldots]\cos^2\phi\, d\sigma\, d\phi\, dz\,, \qquad (4\text{-}69)$$

where

$$(\ldots) = (a\sigma - a\rho'\cos\phi - zz')R^{-1} \qquad (4\text{-}70)$$

and

$$[\ldots] = [\delta(\sigma+\delta\rho) - \delta(a-\delta\rho) - a^{-1}]\,. \qquad (4\text{-}71)$$

After doing the integrals, we have

$$E_x^s(\Phi_1) = i\pi(\kappa-1)a^2\,\delta z\,\delta\rho\, e^{ikR}(R^2\lambda)^{-1}\left(\frac{2}{a}+\frac{ika}{R}\right)J_o\left(\frac{ka\rho'}{R}\right)\mathrm{sinc}\left(\frac{kz'\,\delta z}{R}\right)P'E_o \qquad (4\text{-}72)$$

Note the probe correction P' is $[1 - 3/8\,(\pi^2/4 - 1)\,a^2/R^2]$; it differs from that in Equation (4-67).

The total field is

$$E_x^T = E^I + E_x^s(A) + E_x^s(\Phi) \qquad (4\text{-}73)$$

The observable quantities are intensity $|E_x^T|^2$ and phase, the argument of E_x^T.

This theory does not include the effects of fields reflected from the probe to the scatterer and scattered back to the probe.

The formulas generalize readily to several rings forming a cylinder. For example for two rings

$$E_x^s(A_2) = E^s(A_1)\left(E_{01}\,e^{ikz'\,\delta z/R} + E_{02}\,e^{ikz'\,\delta z\,1R}\right) \qquad (4\text{-}74)$$

where E_{01} and E_{02} are the fields in each of the rings and $E^s(A_1)$ is from Equation (4-67). The scalar potential gives

$$E_x^s(\Phi_2) = E^s(\Phi_2)\left(E_{01}\, e^{ikz'\,\delta z/R} + E_{02}\, e^{ikz'\,\delta z/R}\right) \qquad (4\text{-}75)$$

where $E^s(\Phi_2)$ is from Equation (4-71).

4.5 COMPUTATION

The first example was for a single ring diameter 2a equal λ, length $2\,\delta z = 0.16\,\lambda$, dielectric constant 2.6. Because incidence was axial, necessary conditions on the computed results were that the field at $\phi = 0$ equal that at $\phi = \pi$ and that the field at $\phi = \pi/2$ equal that at $\phi = 3\,\pi/2$. This condition was well satisfied. Figure 4-4 shows computed internal values of E^T for several values of N.

Figure 4-5 shows computed internal values of E^T for a cylinder, diameter λ, length $0.32\,\lambda$. Two rings were utilized.

Figure 4-6 shows computed values of E^T outside the ring, on the z-axis, with and without probe corrections. Figure 4-7 shows computed values of E^T outside the cylinder. Figure 4-8 shows computed values for the cylinder, but the area of the cylinder cross section was reduced by 80% in evaluating the external field integrals,

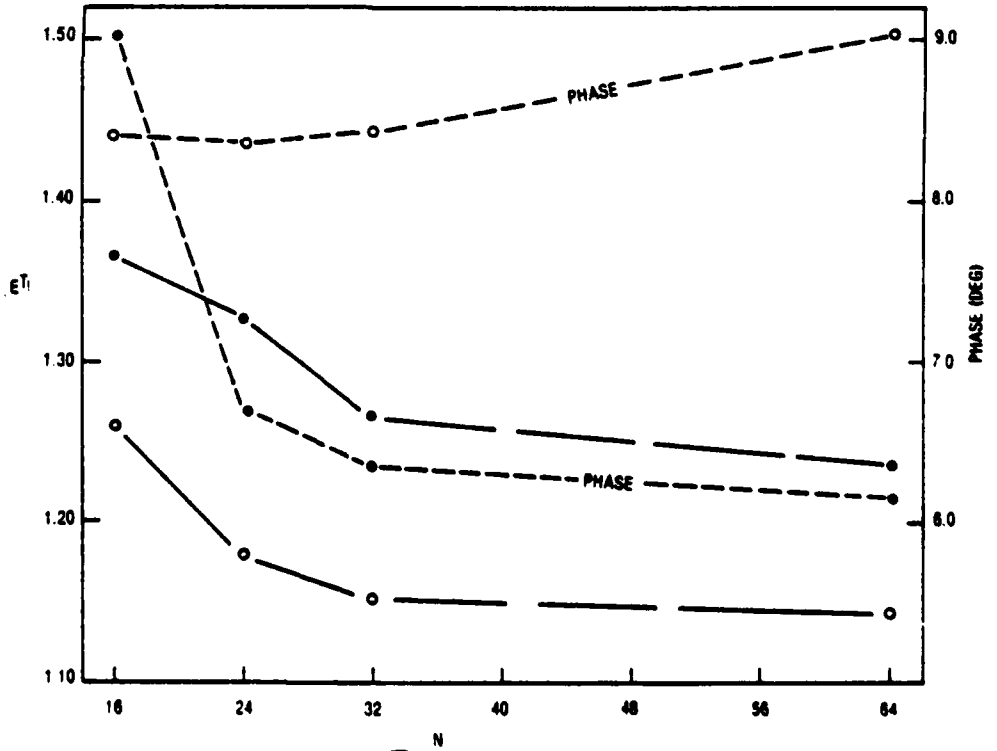

Figure 4-4. Phase and Amplitude of E^T for Single Ring: $\delta z = 0.100$ in., $\delta\rho = 0.030$ in., $x = 2.6$, frequency = 9.375 GHz. For $\phi = 0°$ (o), $\phi = 90°$ (•)

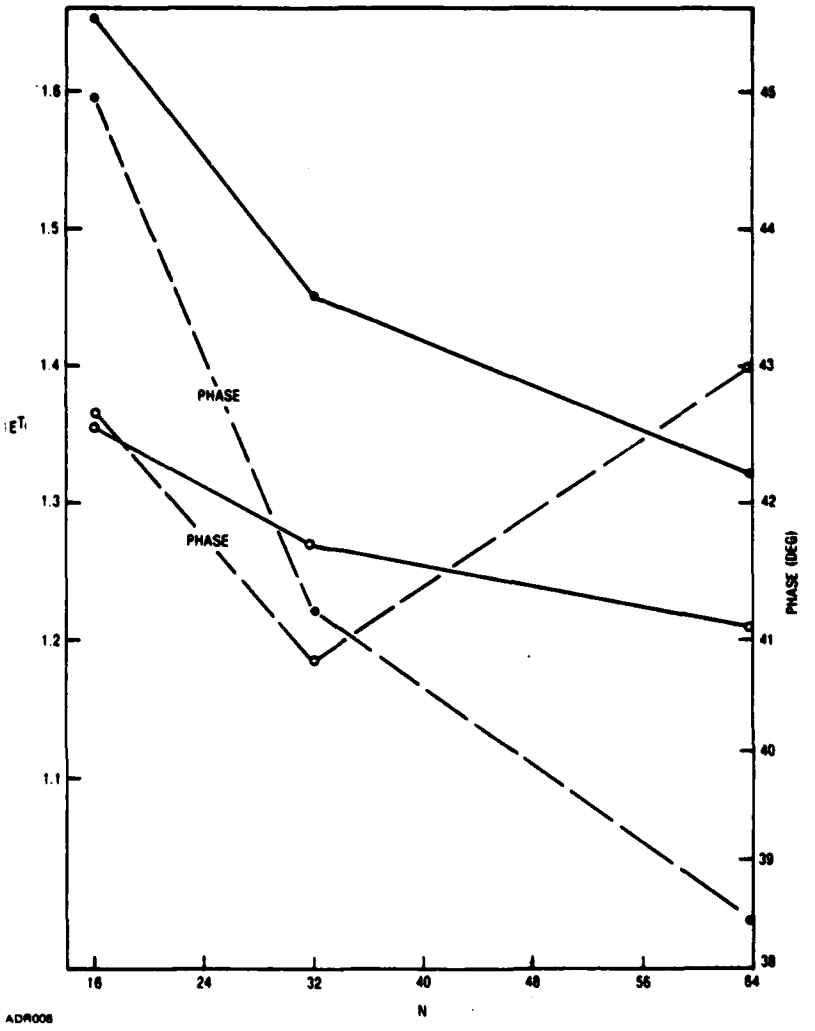

Figure 4-5. Phase and Amplitude of E^T for Two Rings. $\delta z = 0.1045$ in.; $\delta\rho = 0.0313$ in. at center of second cell. Symbols as in Figure 4-4.

Equations (4-74) and (4-75). The area reduction makes the volume of the cylinder equal to that of the elementary integration cells.

4.6 MEASUREMENT

Intensity and phase near the cylinders were measured with a setup that included a travelling half-wave dipole probe and a network analyzer. Measurements were made for horizontal polarization in the system of Figure 4-3. The probe was scanned in the x direction or y direction for fixed values of z. Figures 4-6 and 4-7 show the two observed values on the z-axis; one value comes from each scan.

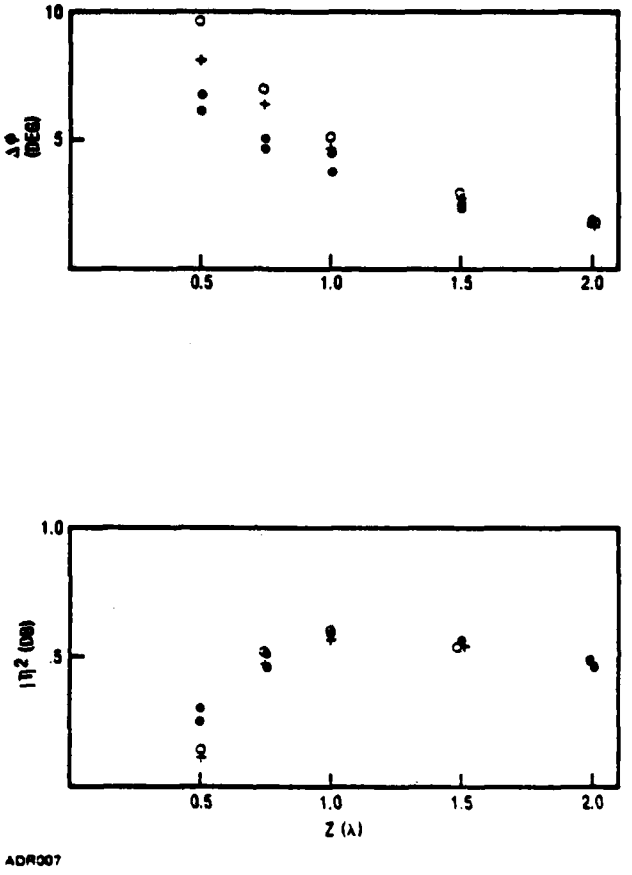

Figure 4-6. **Total Field Behind Dielectric Ring. Length: 0.2 in.; thickness $2\delta\rho$: 0.06 in.; mean diameter 2a: 1.25 in.; dielectric constant 2.6. Measured with dipole probe: (•); computed without probe corrections (o); computed with probe correction (+). Internal field: 1.19 exp i 7.8°. for N = 64**

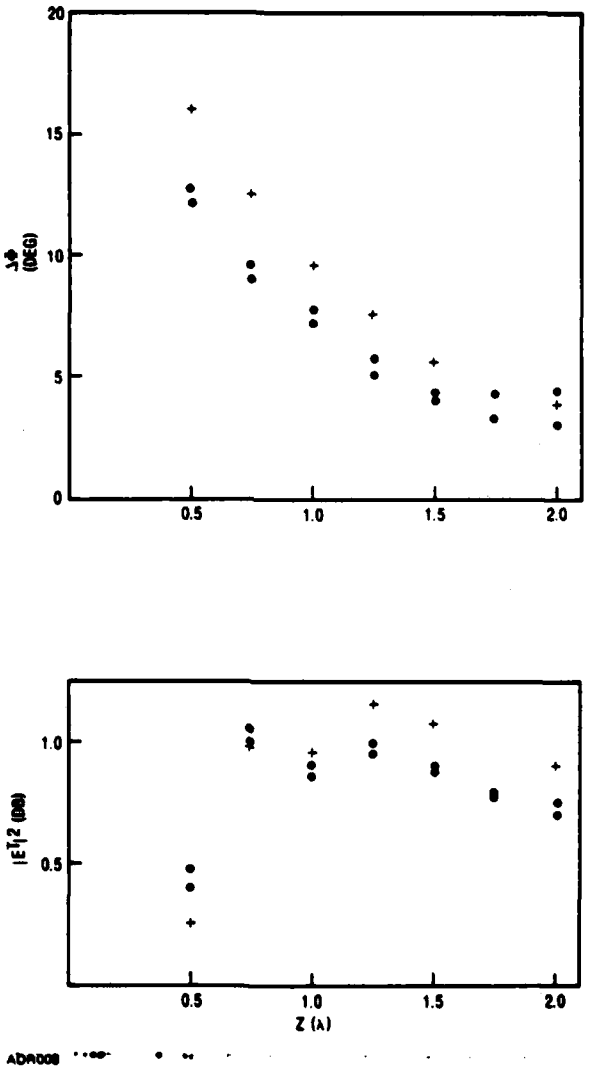

Figure 4-7. Total Field Outside Dielectric Ring. Length is 0.42 in. with other parameters equaling those in Figure 4-6. Measured (•), calculated with probe correction (+)

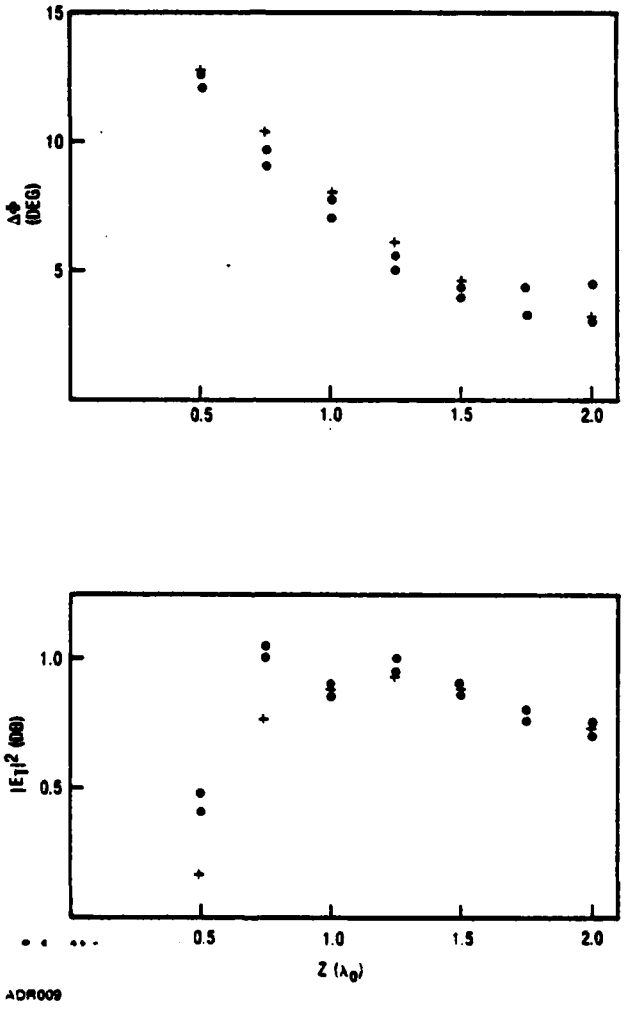

Figure 4-8. As in Figure 4-7 but with $\delta\rho$ Reduced by 20 Percent

5. REFERENCES

1. G. Tricoles, E. L. Rope, R. A. Hayward, "Wave Propagation Through Hollow Dielectric Shells", General Dynamics Electronics Division Report R-77-092-5, November 1978.

2. R. F. Harrington, Time-Harmonic Electromagnetic Fields, McGraw-Hill, pp. 163-168.

3. J. H. Richmond "Scattering by Dielectric Cylinders of Arbitrary Cross Section Shape" IEEE Trans., Vol. AP-13 pp 334-341 (1965).

4. W. K. H. Panofsky and M. Phillips, Classical Electricity and Magnetism, Addison-Wesley, pp 210-215.